CrossMark

ORIGINAL ARTICLE

Post-yield behavior of fixed steel beams encased in concrete with plastic rotation capability under monotonic loads

J. D. Nzabonimpa · Won-Kee Hong · Dinh Han Nguyen

Abstract Flexural strength calculated based on only curvature at sections shows some inconsistencies at large strains compared with nonlinear finite element analyses which considered damaged concrete plasticity. The prediction of the post-yield behavior of steel–concrete composite structures has been a complex issue, rendering analytically inaccurate prediction of the post-yield deflection of composite beams when plastic flows were not considered. The accurate prediction of the post-yield deformation of composite steel beams encased in structural concrete should account for the strain based on plastic rotation. The plastic rotation is influenced by the inelastic energy dissipation. The post-yield behavior of steel–concrete composite structures is affected by the inclination of diagonal cracks of concrete, and the stiffening effect of concrete tension between cracks. Plastic strain occurring in the steel section also contributes to inelastic behavior of composite structures. The aim of this study was to idealize plastic flow of steel beams encased in structural concrete at fixed foundation. Plastic flows were calculated by non-linear finite element analysis including the consideration of concrete plasticity. The post-yield deflection was, then, predicted in a manner reflecting plastic deformation. The proposed idealization agreed well with numerical data obtained by means of nonlinear finite element analysis, providing a simplified but reliable procedure for practicing engineers designing composite structures in the inelastic region.

Keywords Plastic rotation · Steel beams encased in structural concrete · Post-yield deflection · Plastic curvature · Nonlinear finite element analysis · Plastic flow

List of symbols

$G(\sigma)$	Non-associated plastic flow potential, Druker–Prager formulation
σ_{t0}	Uniaxial tensile stress
ε	Eccentricity
ψ	Dilation angle
$\overline{q}$ and $\overline{P}$	Effective stresses
I_1	First stress invariant
J_2	Second deviatoric stress invariant
S	Effective deviatoric stress tensor
$\sigma_{11}, \sigma_{22}, \sigma_{33}$	Principle stresses
K_c	Ratio of the second stress invariant on the tensile meridian to that on the compressive meridian
ε_{st}	Tensile strain of steel at ultimate load limit state

J. D. Nzabonimpa
Department of Civil Engineering, Institut d'Enseignement Superieur de Ruhengeri, P.O.B. 155, Musanze, Republic of Rwanda

W.-K. Hong (✉) · D. H. Nguyen
Department of Architectural Engineering, Kyung Hee University, Yongin 446-701, Republic of Korea
e-mail: hongwk@khu.ac.kr

rilem

ε_{max}	Maximum strain
ε_y	Concrete strain in the extreme compression fiber at yield limit state
ε_c	Concrete strain in the extreme compression fiber at ultimate limit state
ε_{ce}	Concrete strain in the extreme compression fiber when the yield curvature is reached
c	Neutral axis (mm) corresponding to the ultimate limit state
kd	Depth of neutral axis (mm)
F_{ult}	Load at ultimate limit state
F_{max}	Maximum load
f_y	Yield stress of rebar (MPa)
F_y	Yield stress of steel (MPa)
f_{b0}	Initial equibiaxial compressive yield stress
f_{c0}	Initial uniaxial compressive yield stress
f'_c	Concrete compressive strength (MPa)
h	Depth of steel section (mm)
b	Beam width
d	Effective height of beam section (mm)
t_w	Web thickness (mm)
t_f	Flange thickness (mm)
L	Bam length ($L = 1700$ mm)
l_p	Hinge length (mm)
l_{max}	Beam length corresponding to the maximum tensile steel strain (mm)
θ_p	Plastic rotation
z	Distance of critical section to the point of contra-flexure
ρ_s	Ratio of total volume of hoops to total volume of concrete core

1 Introduction

1.1 Problem statements and motivations

Munoz and Hsu [1] performed comparative study, accurately predicting the maximum load capacity and deformation behavior of bi-axially loaded concrete-encased steel column with a pinned-end. In their paper, the post-yield behavior was predicted by the finite difference method to obtain the solution of a system of nonlinear equations. Wang [2] replaced the steel section properties by those of the composite

section, similarly to the British Standard for steel BS 5950 Part 1 [3] to predict column strengths. He also compared them with various predictions and test results, resulting that his methods were conservative with validated accuracy. Fiber section analysis was used by El-Tawil and Deierlein [4] to explore the strength and ductility of the concrete encased composite columns. They assessed the strength and ductility as a function of the ratio of structural steel to gross column area, the compressive strength of concrete, and confinement of concrete by seismic hoop reinforcing. Moment–curvature relationships were presented, however, post-yield deflections based on plastic flow were not provided in this study.

In 2004, the state of the art of nonlinear analysis of steel–concrete composite structures was presented by Spacone and El-Tawil [5] Their collection focused on frame elements, providing faster than continuum finite element models in computation. Powerful approaches including fiber discretization for composite section was introduced with good accuracy. Mirza and Lacroix [6] also provided comparisons of strengths determined from 150 physical tests of rectangular composite steel–concrete columns available in the published literature. They made useful recommendations for the design equations provided by ACI (American Concrete Institute). However, it was not possible to find references among their lists similar to the present study which offers the simplified plastic flow and estimation of the deformations caused by plastic hinges directly. Shanmugam and Lakshmi [7] summarized again extensive research on composite columns with two types, composite columns with steel section encased in concrete, and those with concrete filled steel tube. However, the post-yield behavior of the composite columns influenced by plastic flows and the estimations of plastic deformations were absent even if the state of the arts researches were introduced. In the present study, the simplified plastic flows obtained by idealizing the formation of hinges of the composite sections were proposed to estimate the post-yield behavior and corresponding deflections.

Douglas et al. [8] developed finite elements for a sub-structural model to calculate plastic hinges of RC (reinforced concrete) beams. In their model, the plastic hinge length is increased as strain hardening occurs, enabling good prediction of experimentally measured values. Plem [9] studied the influence of various material properties on the rotation capacity of a plastic

hinge. He used realistic stress–strain curves for the constituent concrete and steel materials. The rotation capacity of a plastic hinge in a RC beam was numerically determined based upon a moment–curvature diagram of the beam section. Researchers have proposed various empirical equations for estimating the equivalent lengths of plastic hinges and the maximum concrete strain at the ultimate limit state for RC beams. Decades ago, Baker [10, 11], Corley [12] and Sawyer [13] proposed empirical formulas to calculate the hinge lengths of reinforced concrete beams. Bachmann [14] proposed a method for calculating the deformations of reinforced concrete flexural members based upon the rotations of elements between cracks rather than based upon the curvature at sections. This method takes into account the effects of crack inclination. In the present study, it was found that analytical evaluation of the behavior in the post-yield region based upon curvature at sections only demonstrated some inconsistencies with numerical results considering concrete plasticity. The plastic rotation of the steel sections integrated with the concrete was not taken into account. Yuan and Wu [15] used a three-dimensional finite element analysis (FEA) method to investigate the behavior of plastic hinges in cyclically loaded RC columns. They proposed a simplified empirical model for the equivalent plastic hinge length under cyclic loading. Investigation of plastic hinges in steel structures has also been conducted. Hoang et al. [16] showed that the rigid–plastic method takes full advantage of mathematical programming achievements in both its analysis and optimization algorithms. Vrouwenvelder [17] described plastic hinges of steel beams based on strain hardening. He proposed plastic hinge equivalent length of 2% of the beam length for the case of restrained cantilever beams. However, sufficient information has not been available to understand plastic hinges and their equivalent lengths to design post-yield deflections of steel beams encased in structural concrete. A major building infrastructure has been built in Quito, Ecuador (Plataforma Gubernamental) which was entirely built with CFT and concrete-encased elements.

1.2 Objectives and research significance (contribution to the prediction of post-yield structural behavior of steel–concrete composite beams)
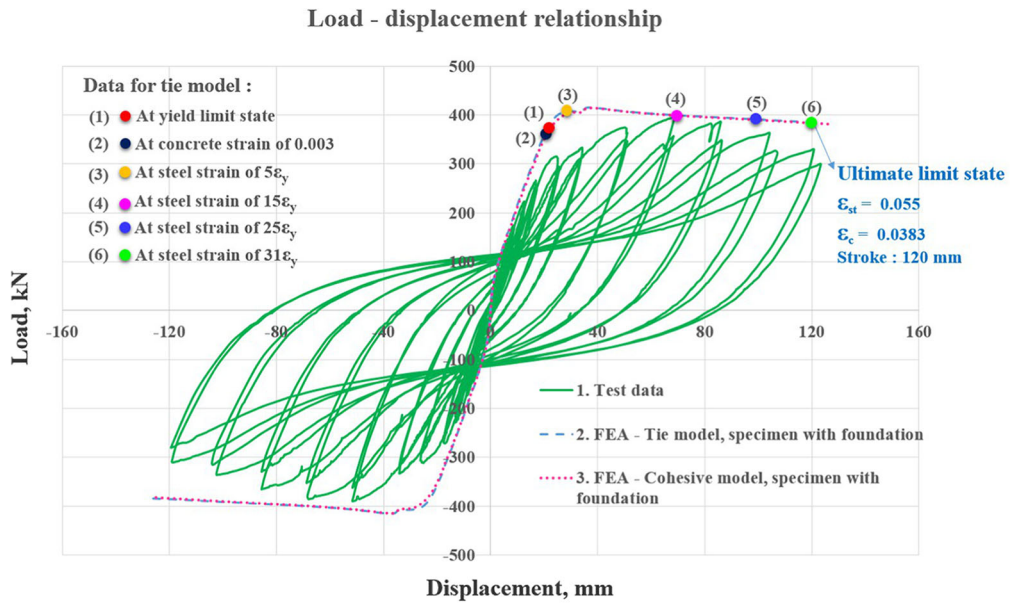
The present work is a post-yield investigation of steel beams encased in structural concrete, aiming to explore the influence of in-elastical behavior upon plastic hinge formation. The presented composite beams utilize the merits of both steel and concrete material without sacrificing performance. Simplified procedures were proposed to estimate post-yield displacement, based on FEA that includes consideration of concrete plasticity.

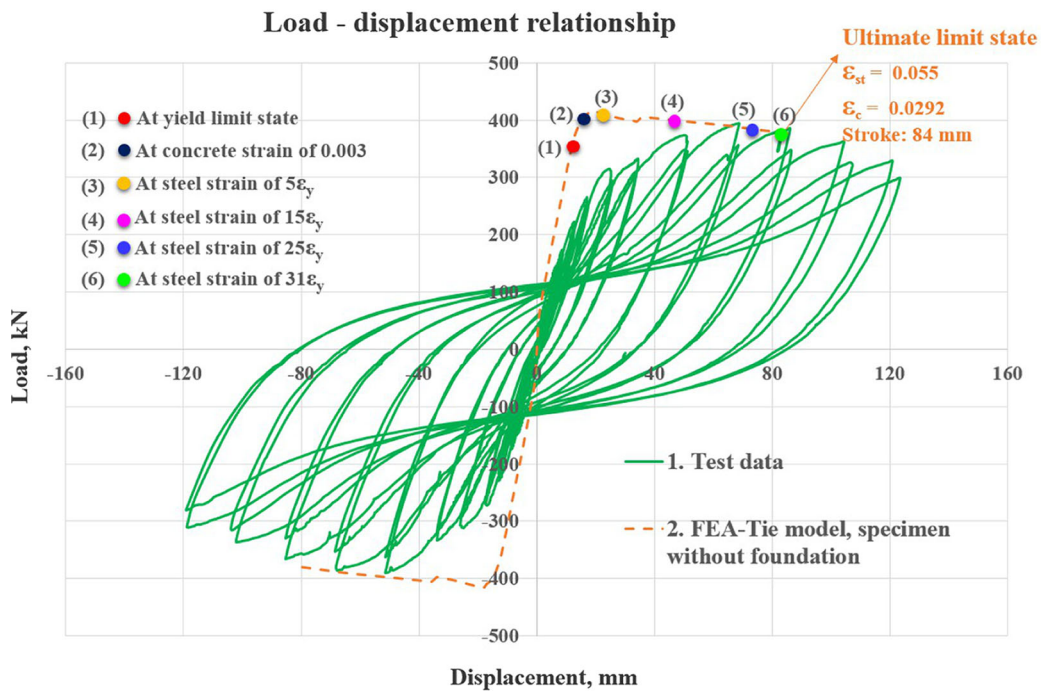## 1.3 Methodology and analysis model

The aim of this study was to idealize the plastic flow of the composite steel beams encased in concrete. The plastic flow of the composite steel beams should be idealized without the rotational components caused by the foundations fabricated for the test. It was, therefore, important to establish the numerical model of composite beams at fixed base to accurately explore the post-yield deflection of composite beams. The rotational components due to the foundation included in the test data had to be removed. For this, the FEA model having the foundation which was included for the test was firstly calibrated to the test data. Once the FEA model with rotational effect was established as shown in Fig. 1a-(1), the foundation was removed from the model to perform another non-linear finite element analysis as shown in Fig. 1a-(2), which was undisturbed by the rotational components due to the foundation. Idealization plastic flow of composite steel beams was, then, followed at varied strain levels from yield limit state up to the ultimate limit state. The load–displacement relationships represented by Legend 2 shown in Fig. 1a-(2) were obtained based on the fixed base. It was obvious that they differ from those observed from the test data because test data contained rotational components. The numerical load–displacement relationships represented by Legend 2 of Fig. 1a-(1) having the rotational influence and Legend 2 of Fig. 1a-(2) without influence of base rotation cannot be compared directly.

In the present study, strain evolution and curvature of four different specimens were explored to develop a method for predicting plastic rotations and equivalent

Load - displacement relationship

Data for tie model :
(1) ● At yield limit state
(2) ● At concrete strain of 0.003
(3) ● At steel strain of $5\varepsilon_y$
(4) ● At steel strain of $15\varepsilon_y$
(5) ● At steel strain of $25\varepsilon_y$
(6) ● At steel strain of $31\varepsilon_y$

Ultimate limit state
$\varepsilon_{st} = 0.055$
$\varepsilon_c = 0.0383$
Stroke : 120 mm

1. Test data
2. FEA - Tie model, specimen with foundation
3. FEA - Cohesive model, specimen with foundation

Displacement, mm

(1) With base rotation; test data included base rotation

Load - displacement relationship

Ultimate limit state
$\varepsilon_{st} = 0.055$
$\varepsilon_c = 0.0292$
Stroke: 84 mm

(1) ● At yield limit state
(2) ● At concrete strain of 0.003
(3) ● At steel strain of $5\varepsilon_y$
(4) ● At steel strain of $15\varepsilon_y$
(5) ● At steel strain of $25\varepsilon_y$
(6) ● At steel strain of $31\varepsilon_y$

1. Test data
2. FEA-Tie model, specimen without foundation

Displacement, mm

(2) Without base rotation (FEA); test data included base rotation

(a)

Fig. 1 Estimation of the maximum tensile strain for various h/d ratios (FEA). **a** Numerical estimation of deflection for 500×500 section. **b** Finite element meshes showing plastic tensile strain of steel section and neutral axis contour for 500×500 section. **c** Load–displacement relationships of various composite sections; FEA specimen without foundation
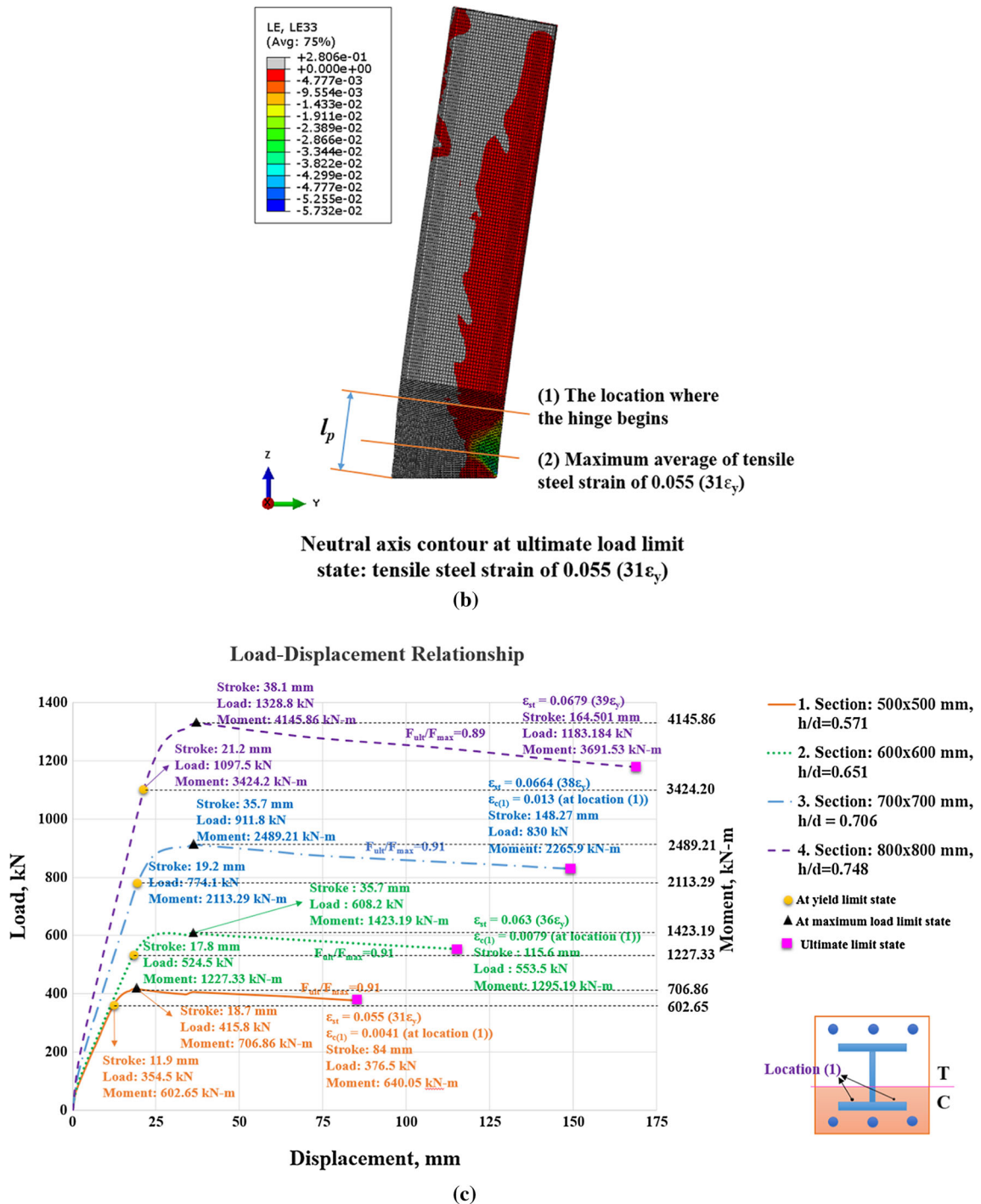
LE, LE33
(Avg: 75%)
+2.806e-01
+0.000e+00
-4.777e-03
-9.554e-03
-1.433e-02
-1.911e-02
-2.389e-02
-2.866e-02
-3.344e-02
-3.822e-02
-4.299e-02
-4.777e-02
-5.255e-02
-5.732e-02

l_p

(1) The location where the hinge begins

(2) Maximum average of tensile steel strain of 0.055 (31ε_y)

Neutral axis contour at ultimate load limit state: tensile steel strain of 0.055 (31ε_y)

(b)

Load-Displacement Relationship

(c)

Fig. 1 continued

hinge lengths by means of nonlinear FEA based on concrete plasticity. Test data obtained from a specimen having a 500 × 500 beam section was used to define the ultimate limit state as shown in Fig. 1a, c. The plastic curvature was idealized, accounting for the inelastic energy dissipation and plastic rotation of

composite beams based upon their ratios of steel section (h) to effective composite beam depth (d). Empirical expressions have been proposed to calculate the maximum strain of steel section embedded in concrete, the equivalent plastic hinge length of the steel section in tension, and the location of neutral axis depth based on the calibrated FE models. The locations of composite sections corresponding to the maximum steel strain and corresponding to where plastic flows began were also idealized. Post-yield deflection of the steel–concrete composite beams was calculated for the ratio of the length of the beam to the effective depth of the composite section of 4.0 and the ratio of volume of confining steel (including the compression steel and rebar) to volume of the concrete core of 0.037. The idealized post-yield deflection was verified by nonlinear FEA, resulting in accurate and rapid prediction of the post-yield behavior of composite beams.

2 FEA of composite beams

2.1 Material parameters in modeling

Table 1 lists the FEA parameters implemented in the nonlinear numerical analysis based on concrete plasticity, including parameters defining the Drucker–Prager hyperbolic plastic potential function and material properties. Equation 1 expresses the Drucker–Prager hyperbolic plastic potential function used in the model of damaged concrete plasticity.

$$G(\sigma) = \sqrt{(\epsilon \sigma_{t0} \tan \psi)^2 + \overline{q}^2} - \overline{p} \tan \psi \qquad (1)$$

The vertical ordinate of the Drucker–Prager hyperbolic plastic potential function represents the von Mises equivalent effective stress, $\overline{q} = \sqrt{\frac{3}{2} S : S} = \sqrt{3 J_2}$, where $J2(J_2 = \sigma_{11}^2 + \sigma_{22}^2 - \sigma_{11} \sigma_{22})$ is the second deviatoric stress invariant for biaxial loading and $S(S = \overline{P}I + \overline{\sigma})$ represents the effective deviatoric stress tensor. The horizontal ordinate represents the hydrostatic pressure, $\overline{P} = -I_1/3 = -(\sigma_{11} + \sigma_{22} + \sigma_{33})/3$. I_1 is the first stress invariant, ψ is the dilation angle measured in the p–q plane under high confining pressure, and σ_{t0} is the uniaxial tensile stress. ε denotes eccentricity. The model of damaged concrete plasticity used in the

present work was constructed based on a non-associated hyperbolic function in which the scalar hardening parameters indicate the length of the strain increment vector. Inelastic strain of a brittle material such as concrete causes considerable volume change by means of a plastic distortion called dilatancy, which is modeled according to the dilation angle in the damaged concrete plasticity model. ABAQUS uses the Drucker–Prager hyperbolic plastic potential function for its concrete plasticity model, in which dilatancy is defined in terms of the dilation angle as described in Eq. 1 [18].

2.2 Description of the finite element model

The FE models introduced in this work were developed based upon continuum elements (8-node linear brick) of type C3D8R [18]. Nonlinear material properties were well represented by these elements. In addition, they are characterized by a constant volume change within each element, preventing mesh locking when the material response is incompressible. A fine mesh of 4 mm was assigned to the beam fixed end, whereas the remainder of the beam was discretized with a coarse mesh of 10 mm. The number of total elements and nodes constructed in the FE model for the composite section of width and depth each 500 mm was 111,584 and 138,740, respectively. Modeling of steel–concrete composite members requires proper definition of the interactions between the surfaces in contact. Two models with cohesive and tie were implemented to describe contact between the concrete and reinforcing bars/H-steels, which is available in ABAQUS. In both the tie and cohesive models, rotational degrees of freedom were allowed between the two materials. The two surfaces, the master and slave surfaces, were chosen as depicted in Fig. 2. The surfaces of the H-steels and reinforcing bars were defined as master surfaces, whereas the concrete surface was defined as a slave surface. Table 1 summarizes the material properties and FE parameters used for the calibration of FE models. K is the ratio of the second stress invariant in the tensile meridian to that of compressive meridian which defines the shape of the yield surface in the three dimensional space, which must satisfy the condition $0.5 < K_c \leq 1.0$.

Table 1 Inputs for finite element models

Material parameters	
Concrete	Compressive strength: 21 MPa (test value)
Rebar (HD25)	f_y (yield-strength) = 550 MPa (test value)
Steel section: H ($250 \times 250 \times 9 \times 14$)	f_y (yield-strength) = 350 MPa (test value)
Stirrups (HD10)	f_y = 400 MPa
Concrete parameters for FEA	
Dilation angle	30°
Eccentricity	0.1
F_{bo}/f_{c0}	1.16
K value	0.6667
Viscosity	0.002

Fig. 2 Finite element formulation; discretization and interactions between rebar, H-steel and concrete (section: 500×500 mm)
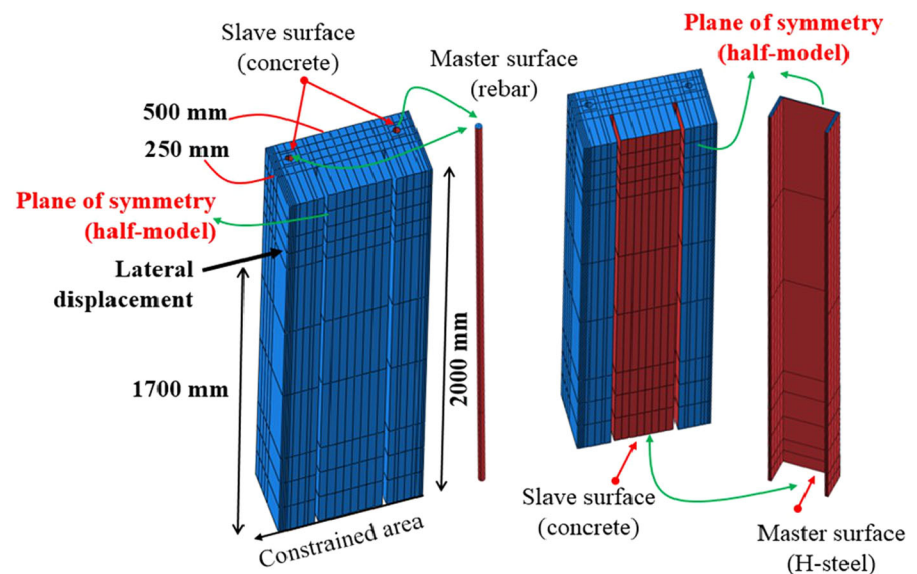
2.3 Calibration of numerical model

Among extensive calibration runs, the numerical model based on tie (Legend 2 of Fig. 1a-(1), with the rotational influence) and cohesive (Legend 3 of Fig. 1a-(1), with the rotational influence) model represented by the load–displacement relationships led to the closest correlation with the test data which contained rotational influence of the base. The instrument-bearing wide flange steel section encased in the structural concrete was tested and shown in Fig. 3. The maximum tensile steel strain of 0.055 in the steel flange of the 500×500 mm composite section was estimated numerically based upon the nonlinear FEA considering concrete plasticity. The ultimate limit state was defined by strain of 0.055 at the deflection of 120 mm (Fig. 1a) [19]. At the ultimate limit state, the ratio of the load at the maximum load limit to the load at the ultimate load limit state was found to be 0.9. The deflection of the specimen due to base rotation was estimated by subtracting the numerical deflection with fixed base corresponding to the steel flange strain of 0.055 (at ultimate limit state) from the total deflection including foundation rotation (Fig. 1a-(1), trace 2). Finite element meshes showing the average strain of 0.055 are shown in Fig. 1b. The numerical deflection reached 120 mm when the deflection due to base rotation was included in the model (Fig. 1a-(1), trace
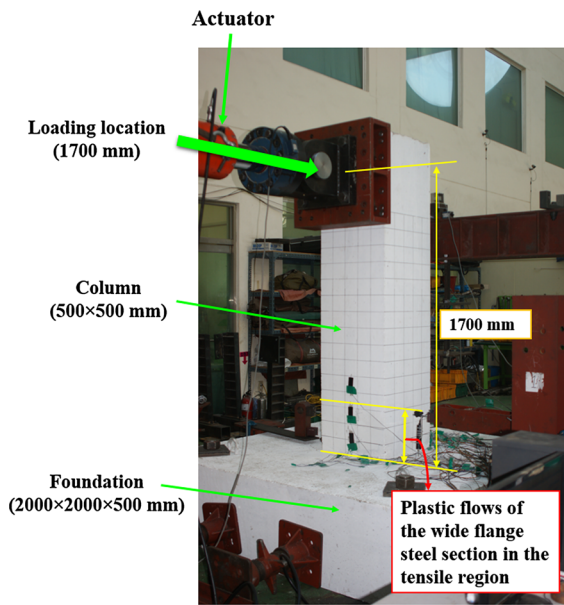
Fig. 3 Test setup and loads [19]

2). Deflection of 84 mm with a fixed base was estimated, corresponding to the steel flange strain of 0.055, when deflection due to rotational components of the base was removed (Fig. 1a-(2), trace 2). Load–displacement relationships for various ratios of depth to effective height (h/d ratios) are presented in Fig. 1c, including the load at the ultimate limit state for each specimen. Table 2 lists properties (coupon test results) of the various sections used for investigating plastic rotation capability.

3 Idealization of plastic flows

3.1 Maximum strain

Plastic rotation for concrete sections in terms of the curvature at an ultimate limit state can be calculated as in Eq. 2 [20], where c is the neutral axis depth, kd is the neutral axis depth at the yield limit state, and ε_c and ε_y are the concrete strain in the extreme compression fiber in the ultimate and yield limit states, respectively.

$$\theta_p = \left(\frac{\varepsilon_c}{c} - \frac{\varepsilon_{ce}}{kd}\right)l_p \tag{2}$$

Various empirical expressions have been proposed for the equivalent length of the plastic hinge and the maximum concrete strain at ultimate curvature for the concrete frames. Corley and Mattack suggested the following expressions for plastic hinge length and the maximum concrete strain at ultimate curvature for concrete members [21]. l_p, d and b represents equivalent hinge length, beam depth, and beam width, respectively. z and ρ_s indicates distance of critical section to the point of contra-flexure and the ratio of total volume of hoops to total volume of concrete core, respectively.

$$l_p = 0.5d + 0.05z \tag{3}$$

$$\varepsilon_c = 0.003 + 0.02\frac{b}{z} + 0.2\rho_s \tag{4}$$

Bachmann [14] calculated the deformation of reinforced concrete flexural members based upon the rotations of the components between cracks rather than

Table 2 Section properties used for numerical investigation

Section (h/d)	Depth of H-steel section (mm)	Effective height of beam section (mm)	Web thickness of H-steel section (mm)	Flange thickness of H-steel section (mm)	Compressive strength of concrete (MPa)	Yield strength of rebar (MPa)	Yield strength of steel (MPa)
	h	d	t_w	t_f	f'_c	f_y	F_y
500 × 500 (0.571)	250	437.5	9	14	21	550	350
600 × 600 (0.651)	350	537.5	10	16	21	550	350
700 × 700 (0.706)	450	637.5	12	18	21	550	350
800 × 800 (0.748)	550	735.5	15	20	21	550	350

the curvature at sections. However, deformation of concrete-encased steel beams due to plastic rotations cannot be estimated by using empirical expressions developed for concrete structures. Concrete undergoing strain confined by both transverse rebar and the steel section contribute more to the load bearing capacity than the case without such confining effects, as studied by Chen and Nan [22]. The hinge lengths should reflect composite actions for the steel section encased in structural concrete too. However, there have been not many reports available on steel beams encased in structural concrete. In the present work, the confining effect by both transverse rebar and the steel section was found to increase plastic rotation of the steel–concrete composite beams. The hinge length of the steel beams encased in structural concrete was estimated based upon FEA including consideration of concrete plasticity. As part of this, the maximum tensile strains of steel sections embedded in concrete were found as 0.055, 0.063, 0.066 and 0.067 for the h/d ratios of 0.571, 0.651, 0.706 and 0.748, respectively. The h/d ratio is the ratio of the depth of the steel section encased in concrete to the effective depth of the composite section. This ratio is one of the parameters that affect the flexural moment capacity of the composite beam. Greater concrete strain can be reached when the concrete is confined by both the transverse reinforcing steels and steel sections. In the numerical analysis, the ratio of the beam length to the effective depth of the composite section was set to be 4.0. The ratio of the volume of confining steel (including the compression steel and rebar) to the volume of the concrete core was also set to be 0.037. The empirical expression was suggested as Eq. 5 below to determine the maximum steel strain that can be reached during the plasticization of the composite section. The maximum tensile strain for the 800×800 section was estimated to be 0.0679 ($39\varepsilon_y$) in this way.

$$\varepsilon_y = -0.2828(h/d)^2 + 0.4456\,(h/d) - 0.1072 \quad (5)$$

3.2 Effect of h/d ratio upon plastic flow (l_p/L, hinge zone)

The plastic flows and hinges responsible for the inelastic deformation of composite beams were estimated based upon FEA including concrete plasticity. The plastic flow increased rapidly at $\left(\frac{l_p}{L}\right)$ because the

rate of strain caused by plastic flows increased substantially due to the plasticization of the sections. The inclination of diagonal cracks of concrete and the stiffening effect of concrete tension between cracks contributed to the plastic flow of the composite sections. In addition to the plastic flow, the inclination of diagonal cracks affect the stiffness, shear and bending deformation of beams, and thus further influence the post-yielding deflection of beams, which were described by Pan et al. [23], Rahal [24], and Hu and Wu [25]. The plastic strains occurring in the steel section during plastic rotations of the sections were also responsible for the rapid rate of plastic flows. The plastic zone was represented by the maximum strain of the section (Fig. 1b, location 2) and the initiated location of plastic hinges (Fig. 1b, location 1). The influence of the depth of the steel section encased in structural concrete upon the plastic flows is presented in Fig. 4a. The numerical results were presented for ratios of the depth of steel section to the effective beam depth (h/d). In the analysis shown in Fig. 4a, the L/d ratio and $\rho_{\text{confining}}$ were 4.0 and 0.037, respectively, where L is the length of the beams and $\rho_{\text{confining}}$ is the transverse steel ratio including compressive rebar and the steel section. The h/d ratio was considered as an important design parameter for the estimation of the in-elastic behavior of the composite beams. The ratio of equivalent plastic hinge length to beam length $\left(\frac{l_p}{L}\right)$ was investigated for three h/d ratios as shown in Fig. 4a. Equivalent plastic hinge lengths of 19, 18, and 19% of the beam length were found for the 500×500, 600×600 and 700×700 sections, respectively. Equation 6 is an empirical expression for the equivalent plastic hinge lengths obtained based on the Fig. 4a results. The equivalent plastic hinge length, l_p, of composite members with an 800×800 section was estimated to be 580 mm by using Eq. 6.

$$l_p/L = -0.009\,(h/d) + 0.1925 \quad (6)$$

3.3 Idealized neutral axes

Neutral axes for all strain levels found by using FEA, except at the yield limit state, exhibited similar for the same h/d ratio of 500×500, 600×600, and 700×700 sections. Finite meshes showing the neutral axis of the 500×500 composite section appear in Fig. 1b. The strains in both compressive and tensile

Ratio l_p/L, c/d - h/d relationship
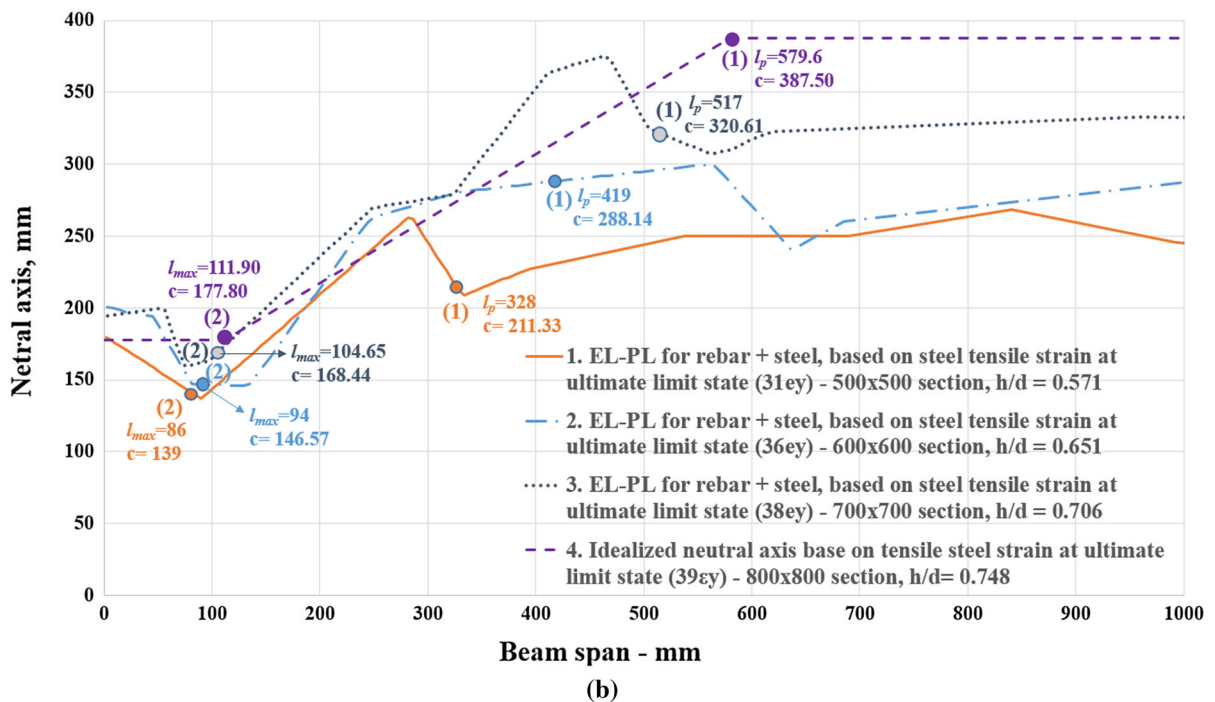

(a)
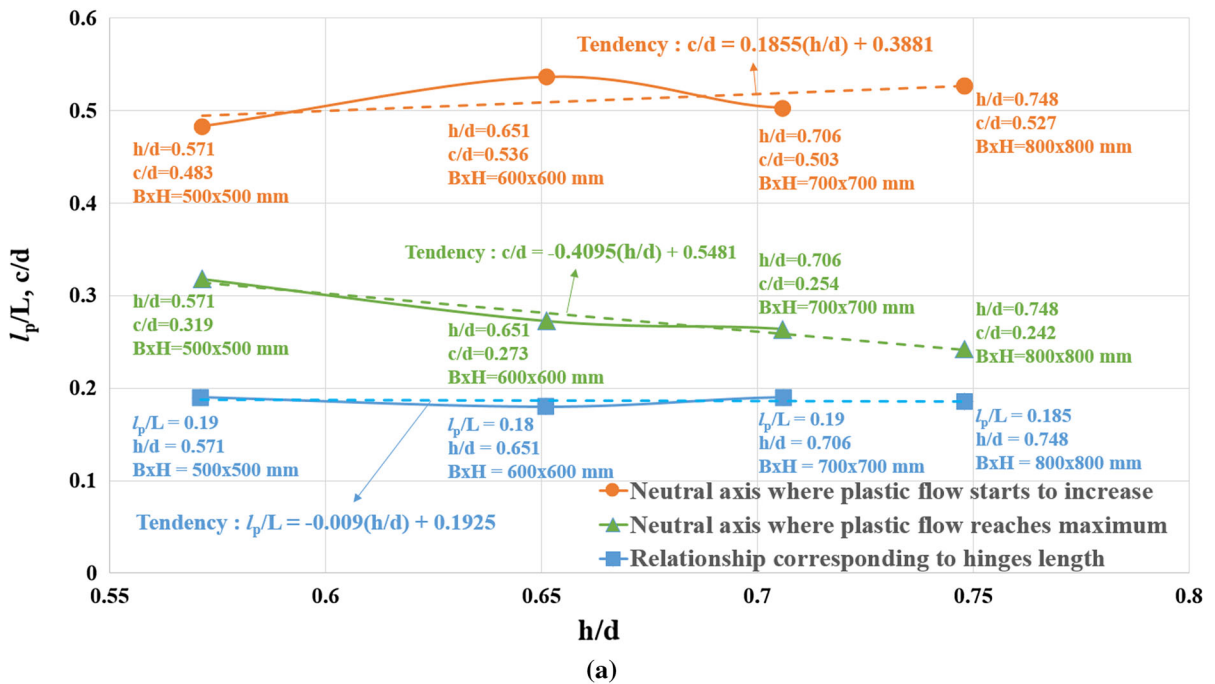
Neutral axis distribution

(b)

Fig. 4 Idealization of the neutral axes corresponding to the location where the maximum strain of the section occurred and plastic flow began. **a** Empirical expression of the neutral axis: c/d versus h/d ratio. **b** Neutral axis profiles for various h/d ratios; tie model without foundation, no damage

zones changed in a manner correlated with each other as the plastic zones extended. The locations where the maximum strain of the section occurred and plastic flow initiated were idealized by Locations 1 and 2, respectively, as indicated in Fig. 1b.

The neutral axes at steel strain of ε_y, $5\varepsilon_y$, $15\varepsilon_y$, $25\varepsilon_y$ and $31\varepsilon_y$ were idealized at Locations 1 and 2. The neutral axes at the initiated locations of plastic flow and at the locations of the maximum strain were shown in Fig. 4b. The neutral axes fluctuated depending on the concrete and steel strain. In Fig. 4b, the neutral axis depths decreased at 282 mm from the fixed end when tensile steel strain increased faster than the compressive concrete strain. However, tensile steel strain decreased rapidly at around 86 mm, followed by a decrease of compressive concrete strain at 26 mm, within the rigid zone between the fixed end and 86 mm. The neutral axes profiles for various h/d ratios are compared in Fig. 4b. Herein; the neutral axes for all strain levels except at the yield limit state were idealized. The ratio of neutral axis depth to effective depth of the section appears in Fig. 4b as a function of the h/d ratio. This information allowed one to develop an empirical equation for locating the neutral axis at Locations 1 and 2. Equation 7 idealized by Fig. 4a is this empirical expression. It can be used to estimate curvature of the composite members. Equations 7.1 and 7.2 respectively represent Locations 1 and 2. The two types of neutral axes for an 800×800 section based on these equations were estimated to be 387.6 and 177.8 mm for Locations 1 and 2, respectively.

$$c/d = -0.4095\,(h/d) + 0.5481 \ \text{ at } \text{ Location } 2 \tag{7.1}$$

$$c/d = 0.1855\,(h/d) + 0.3881 \text{ at Location } 1 \tag{7.2}$$

3.4 The evolution of strain and curvature

Evolution of tensile strain of the steel flange for the section of width and depth 500 mm $\times$ 500 mm was obtained numerically at the steel strain of ε_y, $5\varepsilon_y$, $15\varepsilon_y$, $25\varepsilon_y$ and $31\varepsilon_y$ from the yield to the ultimate limit (Fig. 5a). The strain at Location 2 peaked at the 86-mm beam span. Similar evolutions of tensile strain were observed for 600×600 and 700×700 sections, indicating that the plastic flow can be predicted in terms of the h/d ratio. Location 2, corresponding to

the maximum tensile steel strain embedded in concrete, can be estimated using the empirical expression shown in Fig. 5b. Equation 8 is an empirical formula describing Location 2, developed based upon the Fig. 5b data. This formula is proposed to idealize the curvature of composite members. The location corresponding to the maximum tensile steel strain for an 800×800 section was estimated to be 111.8 mm by using Eq. 8.

$$l_{\max}/d = -0.2446(h/d) + 0.3351 \ \text{ or } \ l_{\max}/L$$
$$= -0.0941(h/d) + 0.1034 \tag{8}$$

4 Idealized post-yield deflections

4.1 Idealization of curvature

The curvature distribution of beams with 500×500 (refer to Fig. 6a), 600×600 and 700×700 cross sections was computed by dividing the tensile strain evolutions of the steel flange at ε_y, $5\varepsilon_y$, $15\varepsilon_y$, $25\varepsilon_y$ (Fig. 5a) by the corresponding neutral axis depths shown in Fig. 4a, b. The ultimate curvature distribution of the steel section in the tension zone was defined by the maximum steel strain for the composite section. In Fig. 6b, plastic curvature is represented based on idealized parameters, with two straight lines defining three locations, the beginning of the plastic rotations, the apex of the curvature corresponding to the maximum strain of the tensile steel section, and straight lines connecting pairs of these points. Plastic curvature of all sections at their ultimate limit states was provided including the curvature of the 800×800 section indicated by the Curvature curve 4 of Fig. 6b. The plastic curvatures were idealized by the maximum steel strain (Location 2 of Figs. 5b, 6b), equivalent plastic hinge length (Fig. 4a), the initiated location of hinge (Location 1 of Fig. 6b), and the neutral axis depth (Fig. 4b) corresponding both to the maximum tensile steel strain and to one plastic flow started increasing, respectively.

At the yield limit state, the curvature (Fig. 6a) and corresponding deflection using neural axis obtained based on strain compatibility yielded the deflection similar to that estimated by FEA considering concrete plasticity. However, at ultimate limit state, the curvatures and corresponding deflections demonstrated

Tensile steel strain distribution

(a)
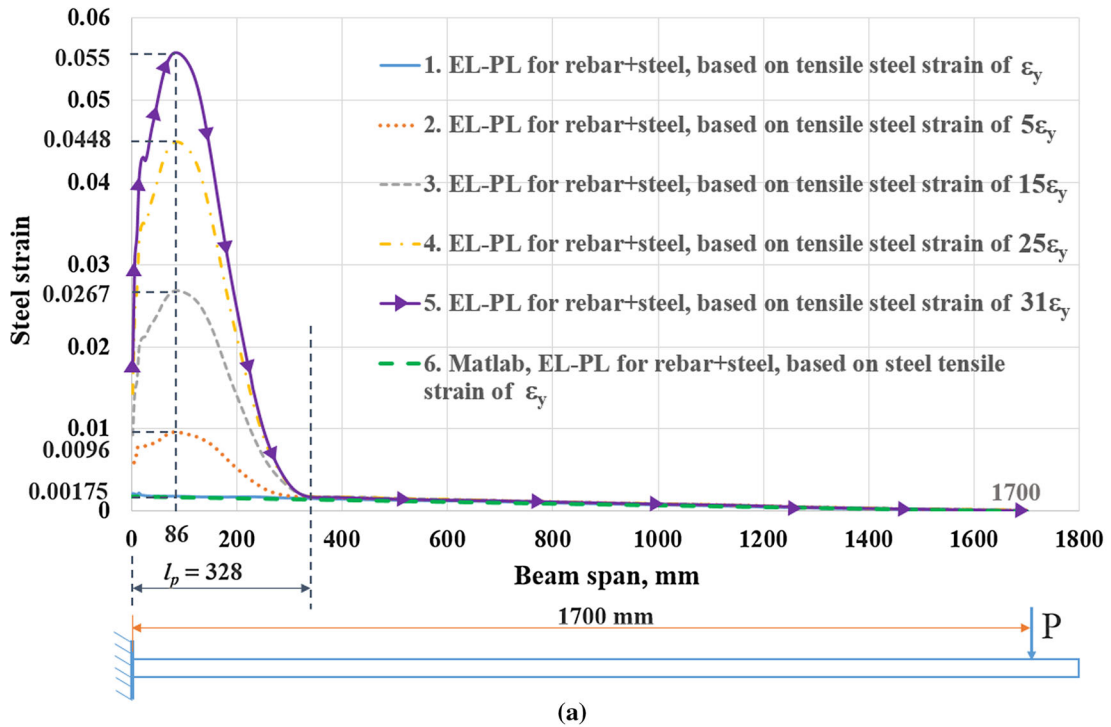
Ratio l_{max}/d, l_{max}/L- h/d relationship
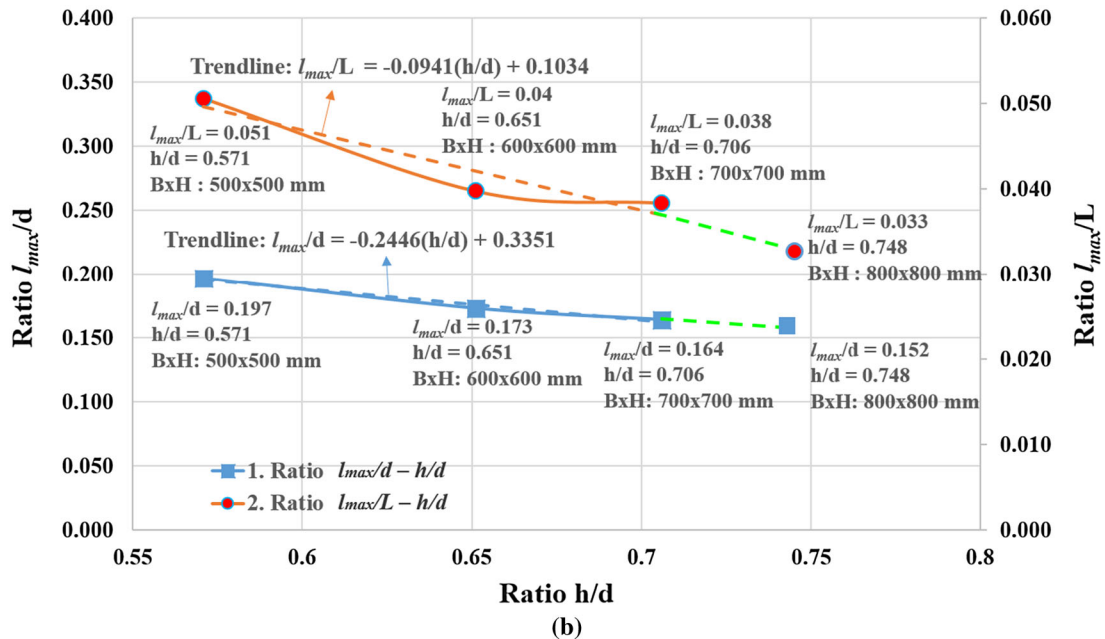

(b)

Fig. 5 Prediction of plastic flow in plastic hinge region. **a** Tensile steel strain; 500×500 section ($h/d = 0.571$); tie model without foundation, no damage. **b** Empirical formula for location corresponding to the maximum tensile steel strain (Location 2)
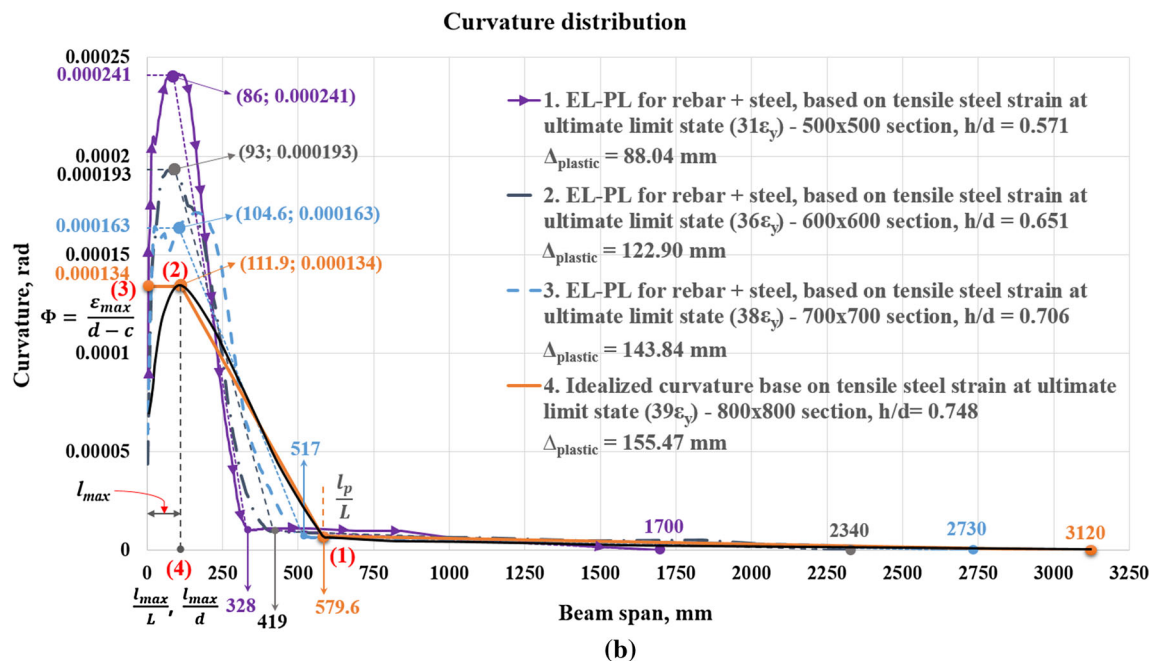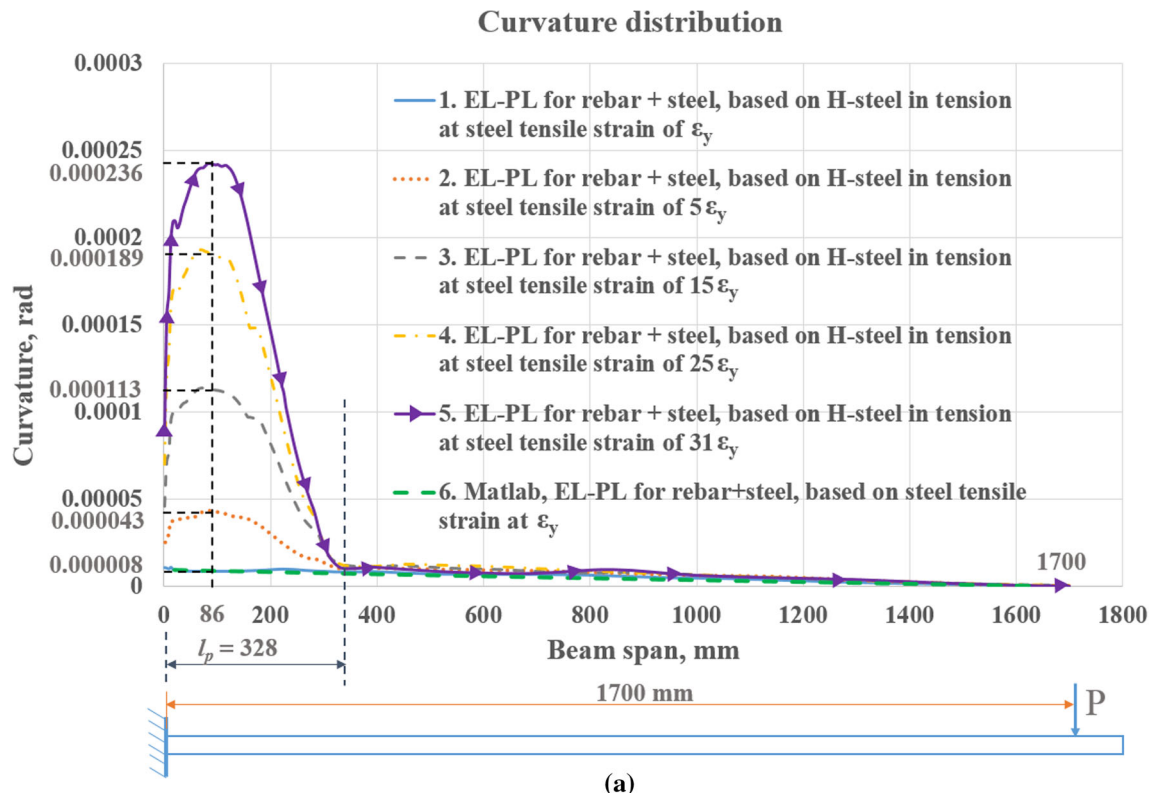
Fig. 6 Plastic curvature of the tensile steel section. **a** Plastic curvature at steel flange at ε_y, $5\varepsilon_y$, $15\varepsilon_y$, $25\varepsilon_y$, and $31\varepsilon_y$ for 500×500 section ($h/d = 0.571$); tie model without foundation, no damage. **b** Idealized plastic curvature for steel beams encased in structural concrete at the ultimate limit state; tie model without foundation, no damage

Table 3 Evaluation of plastic deflection based on plastic rotation

Calculated plastic deformation	At tensile steel strain of ε_y (mm)	At tensile steel strain of $5\varepsilon_y$ (mm)	At tensile steel strain of $15\varepsilon_y$ (mm)	At tensile steel strain of $25\varepsilon_y$ (mm)	At ultimate limit state (mm)
1. Based on idealized tensile steel strain, section: 500×500 mm, $h/d = 0.571$	10.06	22.3	47.31	72.74	88.04
2. ABAQUS, section: 500×500 mm, $h/d = 0.571$	11.9	22.95	47.6	71.4	84
3. Based on idealized tensile steel strain, section: 600×600 mm, $h/d = 0.651$	14.37	27.51	59.68	87.95	122.9
4. ABAQUS, section: 600×600 mm, $h/d = 0.651$	17.85	31.45	61.2	86.7	115.6
5. Based on idealized tensile steel strain, section: 700×700 mm, $h/d = 0.706$	16.07	29.64	65.49	105.82	143.84
6. ABAQUS, section: 700×700 mm, $h/d = 0.706$	19.2	35.7	73.11	107.11	148.3
7. Based on idealized tensile steel strain, section: 800×800 mm, $h/d = 0.748$	17.12	35.44	72.32	107.32	155.47
8. ABAQUS, section: 800×800 mm, $h/d = 0.748$	21.15	43.34	82.69	118.81	164.5

substantial differences as the section became gradually plasticized towards the ultimate limit state. The strain compatibility based neutral axis was also significantly different from the one calculated based FEA considering concrete plasticity. This was because that the neutral axes based on strain compatibility only considered curvature at sections, neglecting curvature caused by concrete plasticity, which was included in the FEA. At the yield limit state, the curvature according to FEA (refer to Legends 1 and 6 of Fig. 6a) agreed well with the curvature computed based on the strain compatibility (considering rotation of the beam section only), without considering inelastic deformation of concrete. FEA considered inelastic deformation of concrete which differed substantially from those calculated without considering concrete plasticity.

4.2 Idealized plastic deflections

The plastic curvature based on the idealized plastic rotation at the tensile steel strain of ε_y, $5\varepsilon_y$, $15\varepsilon_y$, $25\varepsilon_y$, and $31\varepsilon_y$ was used to the estimate plastic deflection of

a 500×500 composite beam. This yielded the deflection of 88 mm, which agreed well with the 84-mm deflection observed in the FEA-based numerical investigation. The plastic deformation based on the actual curvature for the 600×600 section was 114.6 mm, which agreed better with the FEA results (115.6 mm), whereas the plastic deformation based on the idealized plastic flow was 122.9 mm. The plastic deformations of the 700×700 section based on the idealized plastic flow (143.8 mm) were also well correlated with the FEA results (148.3 mm). In Table 3, the plastic deflections estimated based on the idealized plastic flow at the ultimate limit state for all h/d ratios and for the selected steel strains embedded in concrete were compared with those determined by means of FEA considering concrete plasticity. The results demonstrated the simplicity and accuracy of the proposed method in estimating the post-yield deflection of the steel–concrete composite sections.

5 Conclusions

Steel beams encased in structural concrete to reduce floor beam depth were introduced in earlier studies by the present authors without any estimation of the plastic deflections generated by plastic flow of the composite beams. Understanding post-yield structural behavior of composite beams comprising the two entirely different materials, such as structural steel and concrete is quite complicated. A finite element model based on concrete plasticity was developed to estimate the equivalent hinge length and curvature whereas the interface between concrete and steel sections, rebar was modeled based on cohesive contact and tie elements. Post-yield behavior based on the plastic flows caused by the curvature of the compressive concrete and tensile steel flange encased in structural concrete was idealized, being verified numerically. This formulation included consideration of the inelastic energy dissipation based on the inclination of diagonal cracks of concrete, and the stiffening effect of concrete tension between cracks. Plastic strain occurring in the steel section was also considered. Plastic flow and corresponding plastic hinges were idealized based on the load–displacement relationship represented by Legend 2 of Fig. 1a-(2), obtained based on the fixed base. This idealization considered rotational degrees of freedom between concrete and wide flange steel sections. Plastic deformation reflected in the estimation of the post-yield deflection was well correlated with numerical data obtained by nonlinear finite element analysis. A simplified procedure for practicing engineers designing composite structures in the inelastic region was proffered with reliability. Selected findings of this study are summarized below.

1. Numerical investigation of fixed composite beams under monotonic loads based on an FEA was performed to idealize plastic flow of the section. The confining effects provided both by transverse rebars and wide flanges of steel sections encased in structural concrete were considered in this analysis.

2. The neutral axes were idealized based on strains and plastic flows. The stiffness degradation of the composite beams was reflected in the plastic curvature. The ultimate curvature distribution of the composite section in the tension zone was obtained as a function of the maximum strain of steel sections encased in concrete. Inelastic deformation of concrete was not adequately predicted without considering concrete plasticity. However, at the yield limit, the curvature obtained based on the rotation of the beam section without considering inelastic deformation of concrete matched well with the curvature calculated by FEA. This is because the influence of the concrete plasticity is insignificant at the yield limit.

3. A simplified procedure was presented to estimate post-yield deflection of steel beams encased in structural concrete. The confining effect on the concrete contributed by the shear reinforcement and wide flange steel sections were considered in the simplified procedure. The simplified plastic flow was used to explore post-yield behavior of the composite beams with predictable and stable nonlinear structural behavior.

4. The predicted post-yield structural behavior of the composite beams based on the proposed empirical formula agreed well with nonlinear FEA investigation considering concrete plasticity. The applicability to design practice for composite beams was verified with fast and reliable estimation of the post-yield deflection at selected strain levels and h/d ratios.

5. Plastic flow of steel section and concrete either in the compressive or tensile zone can be used to calculate plastic deflections of steel–concrete composite sections. All of curvatures of structural components comprising steel–concrete composite beams can be used to predict post-yield deflections in a rapid and accurate manner, providing design flexibility to support the use of composite beams in practice. For instance, the inelastic curvature distributions of compressive concrete section can be considered for the same results.

6. The proposed method demonstrated the applicability to the design of composite beams, providing fast and reliable prediction of post-yield deflection. A simplified procedure for practicing engineers designing composite structures, in the inelastic region, was proffered with reliability.

Compliance with ethical standards

References

1. Munoz PR, Hsu CT (1997) Behavior of biaxially loaded concrete-encased composite columns. J Struct Eng 123(9):1163–1171
2. Wang YC (1999) Tests on slender composite columns. J Constr Steel Res 49(1):25–41
3. Institution of Civil Engineers (Great Britain). Research Committee (1964) Ultimate load design of concrete structures: report of the [Institution of Civil Engineers] Research Committee with Discussion. Institution of Civil Engineers
4. El-Tawil S, Deierlein GG (1999) Strength and ductility of concrete encased composite columns. J Struct Eng 125(9):1009–1019
5. Spacone E, El-Tawil S (2004) Nonlinear analysis of steel-concrete composite structures: state of the art. J Struct Eng 130(2):159–168
6. Mirza SA, Lacroix EA (2004) Comparative strength analyses of concrete-encased steel composite columns. J Struct Eng 130(12):1941–1953
7. Shanmugam NE, Lakshmi B (2001) State of the art report on steel–concrete composite columns. J Constr Steel Res 57(10):1041–1080
8. Douglas KT, Davidson BJ, Fenwick RC (1996) Modelling reinforced concrete plastic hinges. In: Proceedings of the eleventh world conference on earthquake engineering
9. Plem E (1981) The rotation capacity of plastic hinges in reinforced concrete beams: a theoretical study. Lund Institute of Technology, Lund
10. Baker AL (1956) The ultimate load theory applied to the design of reinforced & prestressed concrete frames. Concrete Publications Ltd., London
11. Baker AL, Amarakone AM (1965) Inelastic hyperstatic frames analysis. Spec Publ Am Concr Inst 12:85–142
12. Corley W (1966) Rotational capacity of reinforced concrete beams. J Struct Div 92(5):121–146
13. Sawyer HA (1965) Design of concrete frames for two failure stages. Spec Publ Am Concr Inst 12:405–437
14. Bachmann H (1971) Influence of shear and band on rotational capacity of reinforced concrete beams. Springer, Berlin, pp 11–28
15. Yuan F, Wu YF (2017) Effect of load cycling on plastic hinge length in RC columns. Eng Struct 147:90–102
16. Hoang VL, Dang HN, Jaspart JP, Demonceau JF (2015) An overview of the plastic-hinge analysis of 3D steel frames. Asia Pac J Comput Eng 2(1):4
17. Vrouwenvelder AC (2003) The plastic behaviour and the calculation of beams and frames subjected to bending. TU Delft, Faculty of Civil Engineering and Geosciences, Delft
18. ABAQUS Analysis User's Manual (2017). Dassault Systèmes Simulia Corp., Providence, RI, USA
19. Hu JY, Hong WK, Park SC (2017) Experimental investigation of precast concrete based dry mechanical column–column joints for precast concrete frames. Struct Des Tall Spec Build 26(5):1–15
20. Park R, Paulay T (1975) Reinforced concrete structures. Wiley, Hoboken
21. Mattock AH (1967) Discussion of "Rotation capacity of reinforced concrete beams" by WG Corley. J Struct Div ASCE 93:519–522
22. Chen CC, Lin NJ (2006) Analytical model for predicting axial capacity and behavior of concrete encased steel composite stub columns. J Constr Steel Res 62(5):424–433
23. Pan Z, Li B, Lu Z (2014) Effective shear stiffness of diagonally cracked reinforced concrete beams. Eng Struct 59:95–103
24. Rahal KN (2010) Post-cracking shear modulus of reinforced concrete membrane elements. Eng Struct 32(1):218–225
25. Hu B, Wu YF (2017) Quantification of shear cracking in reinforced concrete beams. Eng Struct 147:666–678